Journal of Molecular Catalysis A: Chemical 335 (2011) 82–88

Contents lists available at ScienceDirect

Journal of Molecular Catalysis A: Chemical

journal homepage: www.elsevier.com/locate/molcata

Shape effect of ceria in Cu/ceria catalysts for preferential CO oxidation

Jaeman Han[a], Hyung Jun Kim[b], Sangwoon Yoon[b], Hyunjoo Lee[a,*]

[a] Department of Chemical and Biomolecular Engineering, The Specialized Graduate School of Hydrogen & Fuel Cell, Yonsei University, Seoul 120-749, South Korea
[b] Department of Chemistry, Dankook University, Gyeonggi 448-701, South Korea

ARTICLE INFO

Article history:
Received 3 September 2010
Received in revised form
11 November 2010
Accepted 14 November 2010
Available online 21 November 2010

Keywords:
Ceria
Shape
Copper
PROX
Long-term stability

ABSTRACT

Copper was deposited on different shapes of ceria supports (i.e., rods, cubes, and octahedra) and used as catalysts for preferential CO oxidation in excess amounts of hydrogen. When the same amount of copper was deposited, the copper content on the surface measured by X-ray photoelectron spectroscopy differed significantly, with more copper on the ceria octahedra. Copper seemed to migrate into the bulk ceria to a greater degree on the rods. The Cu/ceria-octahedra showed the highest activity of 95% at 140 °C among the three shapes, whereas the Cu/ceria-rods showed higher CO conversion than the Cu/ceria-octahedra at higher temperatures. The Cu/ceria-octahedra showed no activity degradation for CO conversion at 140 °C over 100 h, whereas the activity decreased by 13% for Cu/ceria-rod and 32% for Cu/ceria-cube at the same temperature. The metals Au and Pt were also deposited on the different shapes of ceria, and their activity and selectivity were evaluated.

© 2010 Elsevier B.V. All rights reserved.

1. Introduction

Catalytic properties of activity and selectivity can be controlled by changing the shapes of the catalysts [1,2]. In the case of metallic catalysts, different shapes of nanoparticles have distinct surface atomic arrangements, such as a square arrangement for a {1 0 0} surface, a hexagonal arrangement for a {1 1 1} surface, or a grooved arrangement for a {1 1 0} surface. The change in surface atomic arrangement causes differences in the geometry and binding strength of reactants adsorbed on the surface, resulting in differences in activity and selectivity [3–5]. Metal oxide catalysts with various surface crystalline structures also have different formation energies for oxygen vacancy, leading to differences in oxidation activity. Ceria with different surface crystalline structures, in particular, have been actively investigated [6,7]. The formation and migration of oxygen vacancy and CO adsorption have been estimated for ceria by theoretical simulation [8,9]. For example, when CO is adsorbed on {1 1 0}, {1 0 0}, and {1 1 1} surfaces, a CO molecule bridges two surface oxygen atoms on the surface of {1 1 0} or {1 0 0}, pulling the atoms out of the lattice sites and forming CO_3 species. In this case, the surface structure is deformed due to mild reduction. However, a CO molecule is weakly bound to the {1 1 1} surface, preserving the surface structure [9]. The effect of ceria shape has been investigated for the water–gas shift reaction ($H_2O + CO \rightarrow H_2 + CO_2$) by using gold-deposited ceria rods, cubes, and polyhedra [10]. The rod shape of a ceria nanocrystal has {1 1 0} and {1 0 0} surfaces, the cubic shape has a {1 0 0} surface, and the polyhedral shape mainly has a {1 1 1} surface. CO conversion was evaluated within a range of 150–350 °C. The rod with the smallest oxygen vacancy formation energy showed the highest activity in all ranges of temperature.

Hydrogen, which is the main energy source for fuel cells, has been produced from the water–gas shift reaction or the steam reformation of fossil fuel. In this process, a small amount of CO inevitably remains in the product gas. The residual CO severely poisons the platinum catalyst inside the fuel cell assembly. Therefore, removing CO from hydrogen gas prior to fuel cell operation is essential, and this is usually achieved by the preferential oxidation (PROX) reaction. In the PROX reaction, CO is selectively oxidized to CO_2 in the presence of excessive amounts of hydrogen. Because the oxidation of hydrogen into water is thermodynamically favorable at higher temperatures, the selective CO oxidation can occur at low temperatures [11]. The noble metal catalysts Au, Pt, and Ru have been used to achieve this effect, but high costs hinder their practical use [12–14]. Recently, Cu/ceria was reported to show good results for PROX reactions, and the effects of dopant and nanostructure have been actively investigated [15–20].

In this study, copper was deposited on three different shapes of ceria nanocrystals: rods, cubes, and octahedra. The activity, selectivity and long-term stability of Cu/ceria catalysts with various ceria shapes were evaluated for the PROX reaction. Copper was deposited more on the surface for octahedra while copper seemed to migrate more into lattice for rod. Although oxygen vacancies was formed more on ceria rod, Cu/ceria-octahedra with more surface copper

* Corresponding author. Tel.: +82 2 2123 5759; fax: +82 2 312 6401.
E-mail address: azhyun@yonsei.ac.kr (H. Lee).

1381-1169/$ – see front matter © 2010 Elsevier B.V. All rights reserved.
doi:10.1016/j.molcata.2010.11.017

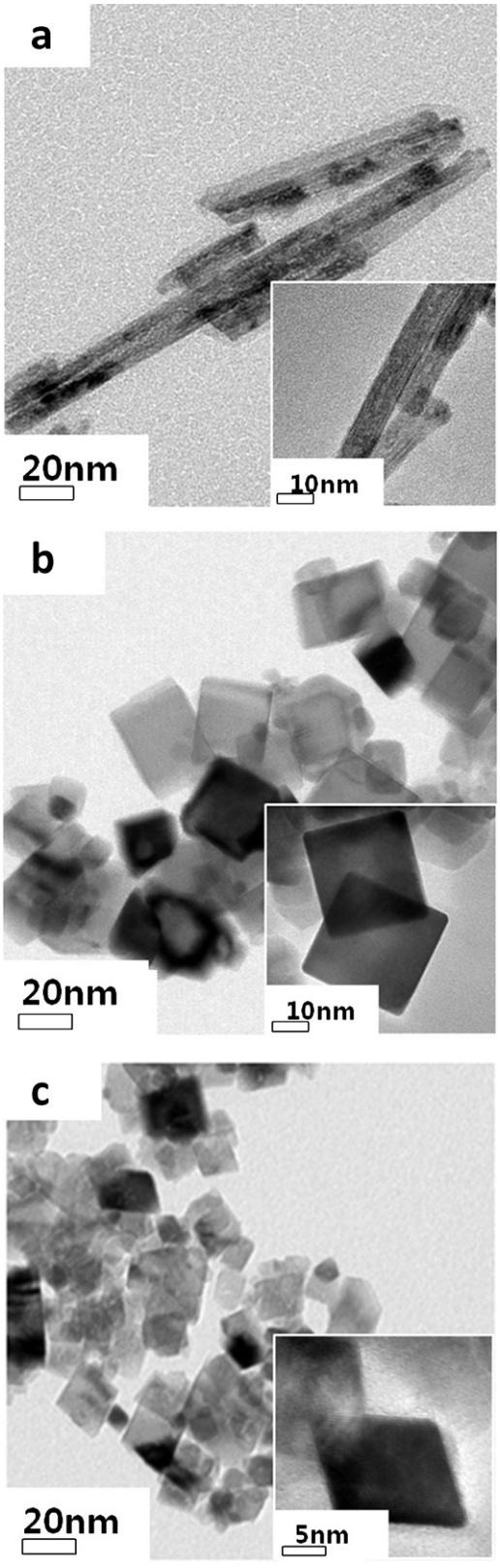

Fig. 1. TEM images of CeO_2 with (a) rod shape, (b) cubic shape, and (c) octahedral shape (the insets are HRTEM images).

and oxygen vacancies similar to Cu/ceria-rod showed the best activity for PROX reaction performed at relatively low temperatures below 150 °C. Additionally, the effect of ceria shape on a long-term stability was evaluated for the first time. Cu/ceria-octahedra showed no degradation over 100 h of PROX reaction while the other shapes demonstrated significant degradation in catalytic activity.

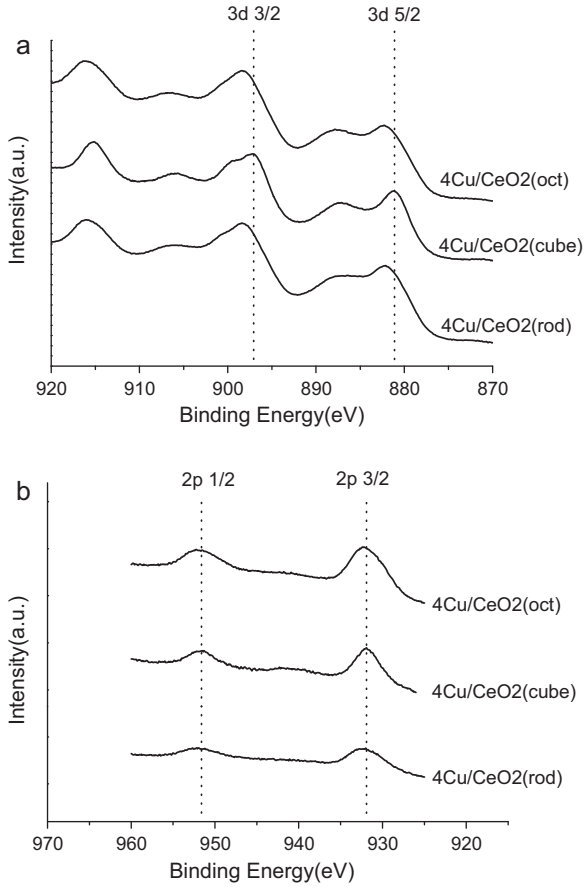

Fig. 2. X-ray photoelectron spectroscopy showing (a) Ce 3d peaks and (b) Cu 2p peaks for 4 wt% Cu/ceria catalysts.

2. Experimental

2.1. Preparation of catalysts

Different shapes of ceria were synthesized by modifying a previously reported recipe [21]. 1.125 mmol of $Ce(NO_3)_3{\cdot}6H_2O$ (Kanto) and 22.5 ml of NaOH (Duksan) solution (6 M for rods; 6 M for cubes; 0.01 M for octahedra) were mixed and continuously stirred for about 30 min. Next, a Teflon bottle containing this mixture was held in a stainless steel autoclave, and the autoclave was sealed tightly. The autoclave was subjected to hydrothermal treatment at different temperatures (100 °C for rods; 180 °C for cubes; 180 °C for octahedra) for 24 h. The obtained precipitates were separated by centrifugation, washed with DI water, and then dried at 80 °C in a vacuum oven overnight. The powders were calcined in air at 400 °C for 4 h. To obtain the Cu/ceria, ceria powder (0.1 g) was slurried in 3 ml of deionized (DI) water. Then a 1, 4 or 10 wt% aqueous solution of $Cu(NO_3)_2{\cdot}3H_2O$ (Aldrich) was added to the above solution dropwise and was continuously stirred for 1 h. Next, 1 M of Na_2CO_3 (Aldrich) solution (molar ratio; Cu precursor:Na_2CO_3 = 1:50) was added dropwise to the solution and stirred for 1 h. The pH value was kept at 8–10. The obtained precipitates were then separated by centrifugation, washed with DI water at 60–70 °C, and then dried at 80 °C in a vacuum oven overnight. The powders were calcined in air at 400 °C for 4 h. The metal precursor and precipitating agent were $HAuCl_4{\cdot}6H_2O$ (Aldrich) and $(NH_4)_2CO_3$ (Aldrich) for Au/ceria, and $(NH_4)_2PtCl_6$ (Aldrich) and $NaBH_4$ (Aldrich) for Pt/ceria.

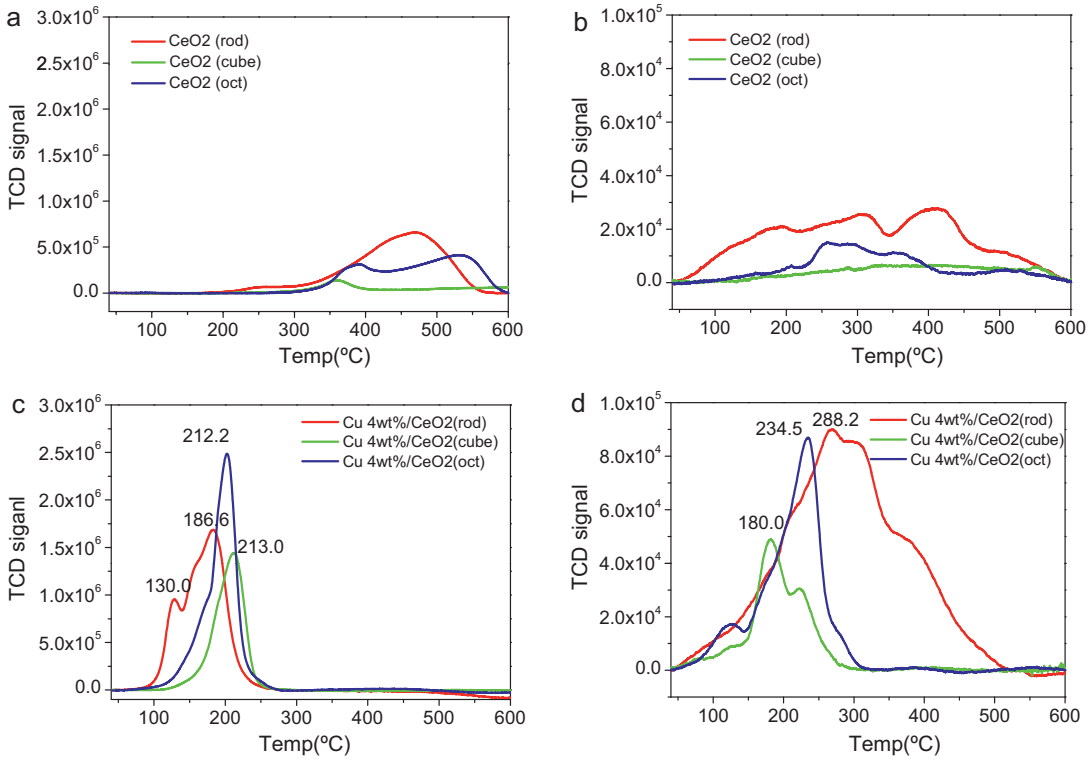

Fig. 3. H_2-TPR profiles of (a) CeO_2 and (c) 4 wt% Cu/CeO_2, and CO-TPR profiles of (b) CeO_2 and (d) 4 wt% Cu/CeO_2.

2.2. Measurements

Transmission electron microscopy (TEM) and high resolution (HR) TEM images were performed with a Tecnai 20 operated at 200 kV. X-ray photoelectron spectroscopy (XPS) data were acquired with a Thermo MultiLab 2000 system. All spectra were collected using Al Kα radiation (1486.6 eV) from a twin anode. High-resolution spectra averaged over 20 scans with a dwell time of 50 ms in steps of 0.1 eV were obtained. The binding energy was referenced with C (1s) at 284.98 eV. H_2 temperature programmed reduction (TPR) and CO-TPR were carried out by a BELCAT-M instrument (BEL Japan, Inc.) using a thermal conductivity detector. Forty milligrams of the catalysts were pre-oxidized in a 20% O_2/He gas mixture at 400 °C for 30 min, and the TPR measurements were performed with a 5% H_2/Ar gas mixture or a 5% CO/He gas mixture with a flow rate of 30 ml/min from room temperature to 600 °C. The temperature increased with a ramping rate of 10 °C/min. Raman spectra were acquired by excitation of the sample at 785 nm using a Raman microscope system (Kaiser, Raman MicroProbe). The spectral resolution corresponded to 4 cm^{-1}. The elemental analysis was performed with inductively coupled plasma (ICP; IRIS Intrepid II, Thermo Elemental).

The PROX reaction was carried out in a quartz glass fixed-bed reactor at atmospheric pressure. A total of 100 mg of catalyst and 400 mg of sea sand were mixed and deposited inside the reactor. The inlet gas flow had a composition of 50% H_2, 1% O_2, 1% CO and He in balance. The total flow rate was 60 ml/min. Before the PROX tests, the catalysts were pre-oxidized in a 10% O_2/He gas mixture at 400 °C for 1 h. The compositions of the effluent gases were measured with an on-line gas chromatograph (GC; Younglin GC 6000 series) equipped with a thermal conductivity detector and a flame ionization detector with methanizer. A 5A molecular sieve and Porapak N were used as a GC column. The CO conversion and selectivity values were calculated as follows:

$$\text{CO conversion}\,(\%) = \frac{[\text{CO}]_{\text{in}} - [\text{CO}]_{\text{out}}}{[\text{CO}]_{\text{in}}} \times 100$$

$$\text{Selectivity}\,(\%) = \frac{0.5([\text{CO}]_{\text{in}} - [\text{CO}]_{\text{out}})}{[\text{O}_2]_{\text{in}} - [\text{O}_2]_{\text{out}}}$$

3. Results and discussion

Fig. 1 shows rod, cube, and octahedral shapes of the ceria nanocrystals. The shapes of each nanocrystal were seen more clearly in the high resolution TEM images of the insets of Fig. 1. These shaped nanocrystals provide distinct {1 1 0} and {1 0 0} surface structures for rods, a {1 0 0} surface for cubes, and a {1 1 1} surface for octahedra. The mean particle size was estimated as 8.7 nm for rods (width), 39.5 nm for cubes, and 15.3 nm for octahedra from peaks at 28.5° in X-ray diffraction patterns by using the Scherer equations. The lengths of the rods were estimated to be 20–200 nm from the TEM images. When 4 wt% of copper was deposited on the various shapes of ceria support, copper nanoparticles were not observed in the TEM images or XRD patterns. Inductively coupled plasma (ICP) elemental analysis showed that the actual amount of deposited copper was 3.9 wt% for rods, 3.9 wt% for cubes, and 4.2 wt% for octahedra. These results suggest that the deposited copper was finely dispersed on the ceria.

The XPS results in Fig. 2 also show that most of the copper occurred as a reduced copper species, not as CuO, due to the absence of shake-up peaks that were expected for Cu^{2+} at 939–944 eV [22]. Highly dispersed CuO_x species in proximity to Ce (Ce–O–Cu sites) are usually considered active sites for CO oxidation, while H_2 oxidation is promoted by partially reduced copper oxide nanoparticles (Cu–O–Cu sites) [23–25]. When the Ce 3d and Cu 2p peak positions in the XPS results were compared, the binding energy of the Cu/ceria-cubes had the lowest value, whereas the Cu/ceria-rods

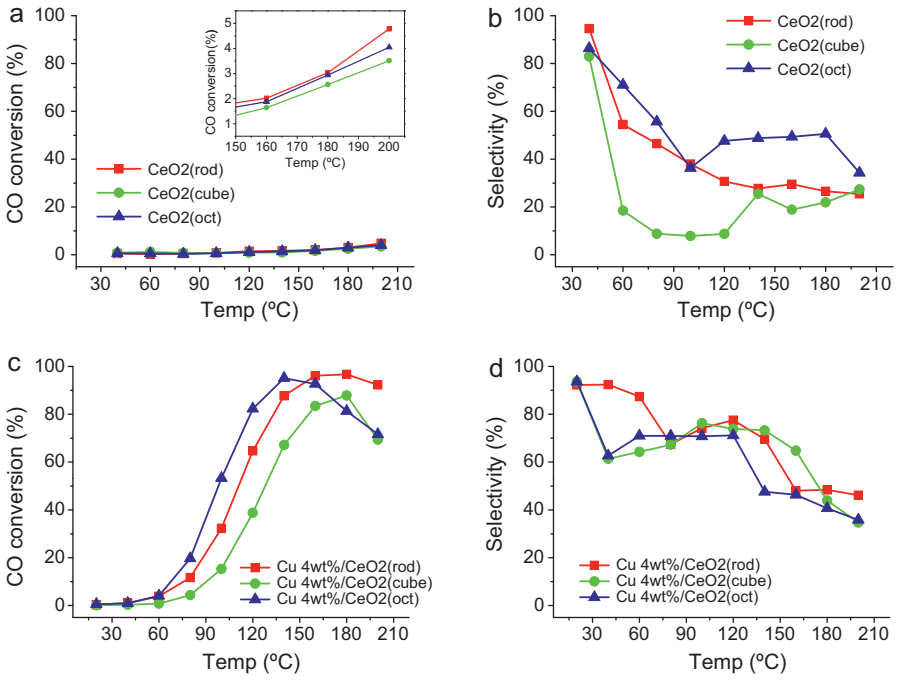

Fig. 4. CO conversion (a and c) and selectivity (b and d) of CeO_2 and 4 wt% Cu/CeO_2 in the PROX reaction (space velocity = 36,000 ml/g catalyst h).

or Cu/ceria-octahedra showed higher binding energies. This result implies that ceria with rod or octahedral shapes have stronger interactions with copper than ceria with a cubic shape. When the Cu/(Cu + Ce) ratio was calculated from the surface atomic contents measured by XPS, the Cu/ceria-rods had the lowest value of 0.21, compared to 0.24 of the Cu/ceria-cubes and 0.35 of the Cu/ceria-octahedra. The surface content of copper was much lower on the rods than the octahedra. The change in surface copper content was also reported for Cu/ceria reduced in different temperatures, which was attributed to the migration of copper into the bulk ceria [25]. Based on the similar amount of copper measured by ICP elemental analysis, the copper seemed to migrate inside the ceria nanocrystal more for the rod than the other shapes. By controlling the shape of the ceria support, the mode of copper deposition into the ceria crystals can be changed, and these changes will affect the activity and selectivity of the PROX reaction.

The H_2-TPR for bare ceria in Fig. 3(a) shows that the surface oxygen was reduced above 300 °C, but the reducing temperature greatly decreased after the copper deposition, as shown in Fig. 3(c). When 4 wt% of copper was deposited, the Cu/ceria were reduced by hydrogen at a temperature range of 185–210 °C. The peak area of the Cu/ceria-cubes was the smallest. The Cu/ceria-rods and Cu/ceria-octahedra had similar peak areas. The Cu/ceria-rods showed a relatively broad peak, implying that different kinds of

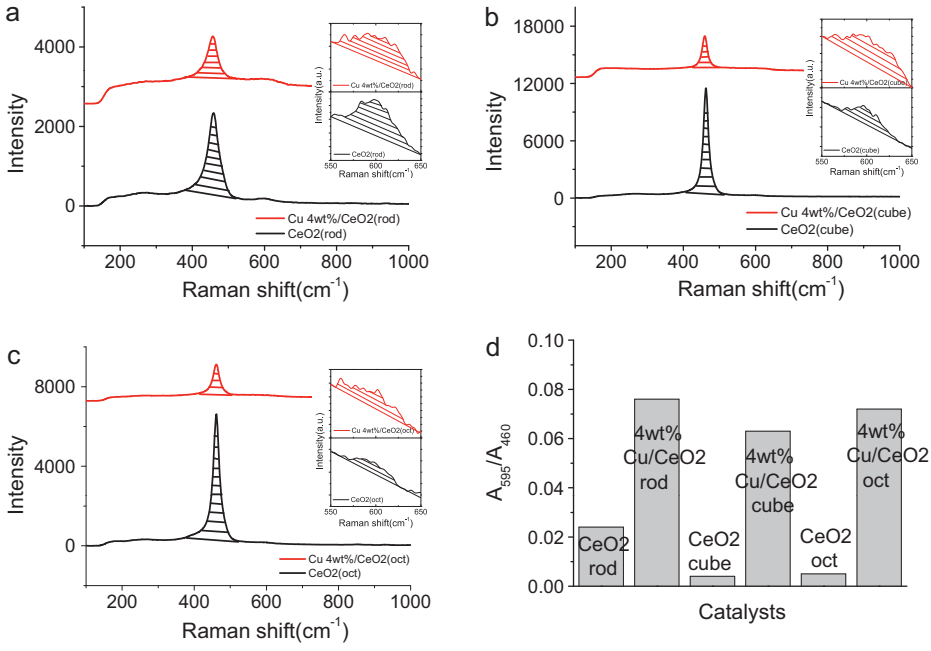

Fig. 5. Raman profiles for a (a) rod shape, (b) cubic shape, (c) octahedral shape, and (d) A_{595}/A_{460} ratio of CeO_2 and 4 wt% Cu/CeO_2.

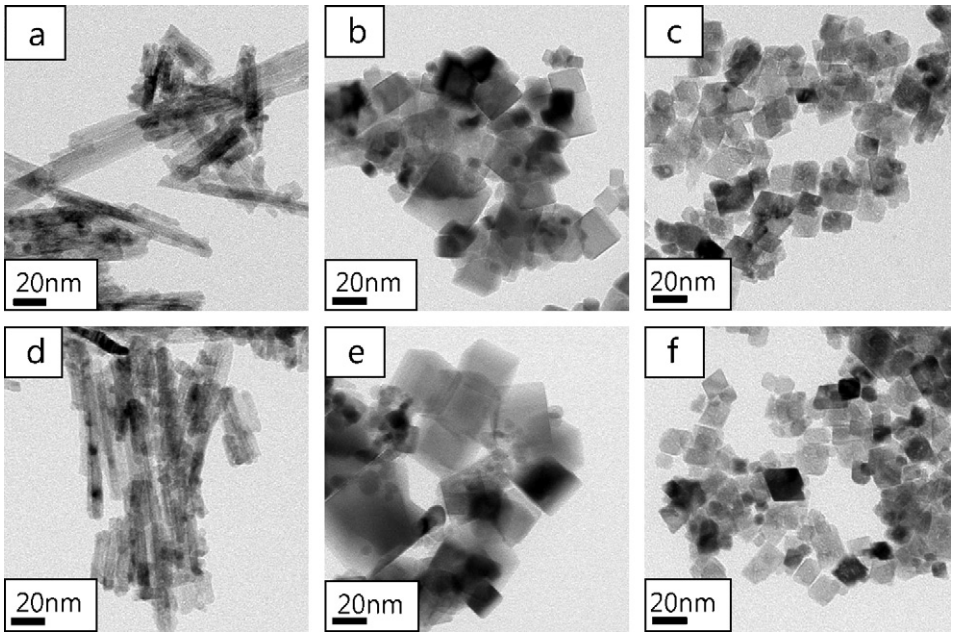

Fig. 6. TEM images of (a) 4 wt% Cu/ceria-rods, (b) 4 wt% Cu/ceria-cubes, and (c) 4 wt% Cu/ceria-octahedra before PROX reaction and (d) 4 wt% Cu/ceria-rods, (e) 4 wt% Cu/ceria-cubes, and (f) 4 wt% Cu/ceria-octahedra after PROX reaction.

reducing sites co-existed. Because a rod consisted of {1 1 0} and {1 0 0} surfaces while the other shaped ceria consisted of either {1 1 1} or {1 0 0}, the interaction of copper on the rod surface would be more diverse. Fig. 3(b) and (d) shows the CO-TPR results of the bare ceria and 4 wt% Cu/ceria, respectively. While the bare ceria showed very broad reduction peaks over a wide range of temperatures with small intensities, the CO consumption was greatly increased after copper deposition. It was recently reported that CO is adsorbed strongly on Cu/CeO_2 (1 1 1) surfaces while CO is only weakly physisorbed on bare CeO_2 (1 1 1) surfaces, based on a theoretical simulation using density functional theory [26]. The amount of CO consumption varied for the different shapes of ceria. The Cu/ceria-rods and Cu/ceria-octahedra showed 4.9 and 1.8 times more CO consumption, respectively, than the Cu/ceria-cubes. Although the Cu/ceria-rods and Cu/ceria-octahedra showed similar peak areas for H_2-TPR, the Cu/ceria-rods had much larger peak area than the Cu/ceria-octahedra, especially in high temperatures above 250 °C. It has been suggested that copper deposited on ceria surfaces exists as CuO, doped Cu^{2+} ions incorporated in the ceria lattice, or surface Cu^{+} ions, and that doped Cu^{2+} ions facilitate oxygen vacancy formation, thus enhancing CO oxidation [26,27].

Because the Cu/ceria-rods had a smaller amount of copper on the surface although total amount of copper was similar, the Cu/ceria-rods would have more doped copper inside the ceria crystal. These doped coppers might move back to the surface, enhancing CO consumption at high temperatures. However, the CO consumption

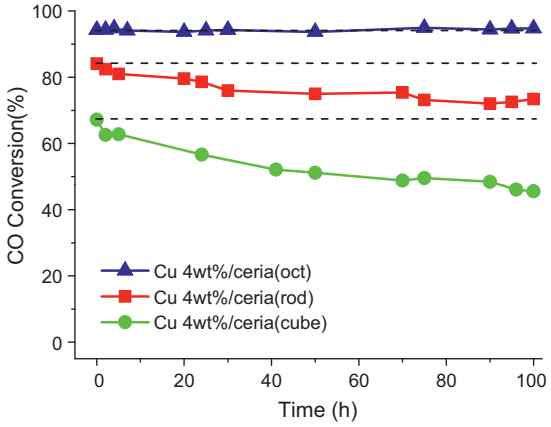

Fig. 7. Long-term stability test for PROX reaction over 4 wt% Cu/CeO_2 at 140 °C.

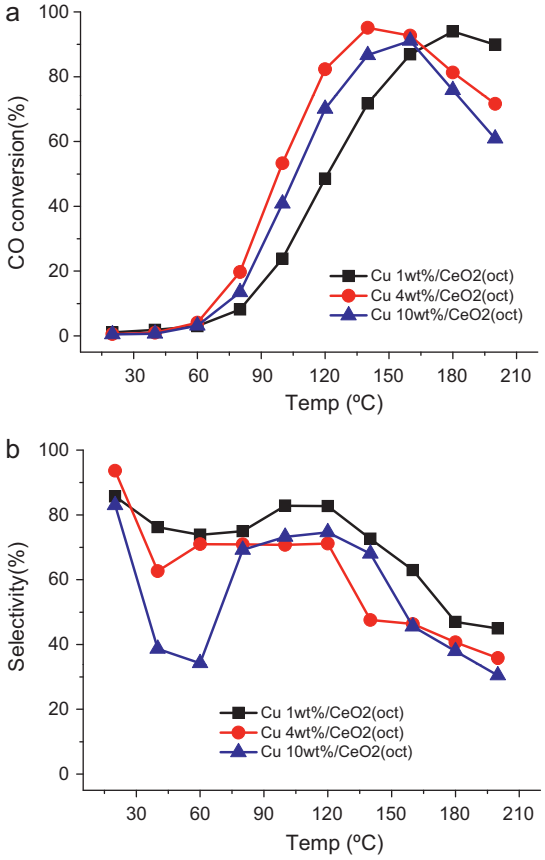

Fig. 8. Effect of copper contents on PROX reaction: (a) activity and (b) selectivity.

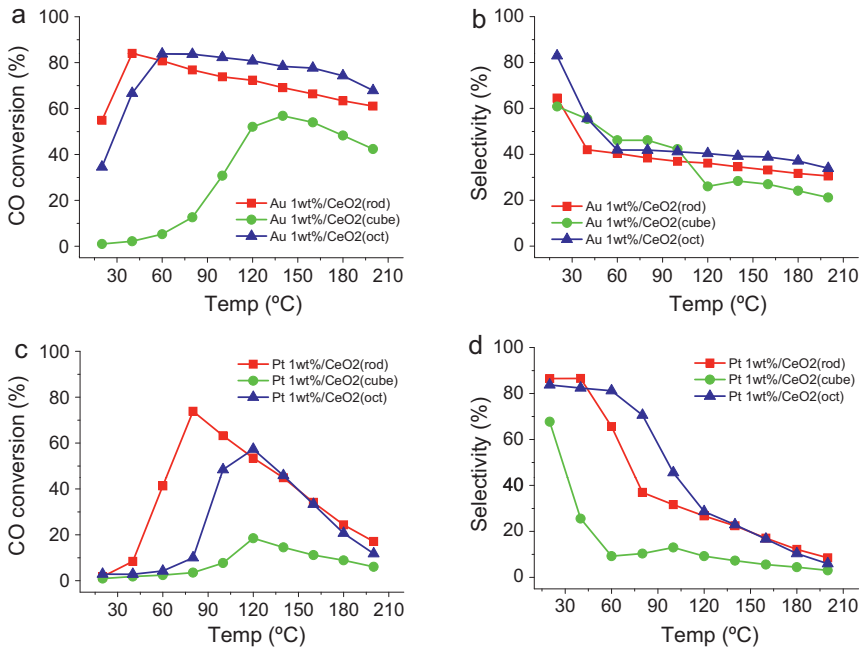

Fig. 9. (a) Activity and (b) selectivity for 1 wt% Au/CeO_2 and (c) activity and (d) selectivity for 1 wt% Pt/CeO_2 in PROX reaction.

in low temperatures below 250 °C was higher for the Cu/ceria-octahedra than the Cu/ceria-rods, probably due to more copper on the surface.

Fig. 4 shows the activity and selectivity for the PROX reaction. The PROX reaction was performed in a gas flow containing 50% H_2, 1% O_2, 1% CO, and He in balance with a space velocity of 36,000 ml/g catalyst h. For the bare ceria, the activity was as low as <5%. The rods showed the highest activity among the shapes, but the difference was minimal. The selectivity, which is a ratio of the oxygen used for CO conversion to the total consumed oxygen, also varied, with the highest selectivity for octahedra and the lowest selectivity for cubes. For the 4 wt% Cu/ceria catalyst, the Cu/ceria-octahedra showed the greatest CO conversion of 95% at 140 °C. The conversion was 87% for the Cu/ceria-rods and 67% for the Cu/ceria-cubes at the same temperature. The reaction rate at 140 °C was calculated as 4.7 μmol/g catalyst s for the Cu/ceria-octahedra, 4.3 μmol/g catalyst s for the Cu/ceria-rods, and 3.3 μmol/g catalyst s for the Cu/ceria-cubes. However, as the temperature increased above 140 °C, the Cu/ceria-rods showed the highest CO conversion while the conversion for the Cu/ceria-octahedra rapidly decreased.

A previous report showed that when gold was deposited on rod, cubic, or polyhedral shapes of ceria, the Au/ceria-rods had the best activity for the water–gas shift reaction at 150–350 °C [10]. The difference in activity for the various shapes was explained by oxygen vacancy formation. Because the formation energy for oxygen vacancy has an order of {1 1 0} < {1 0 0} < {1 1 1} for ceria [8], the rods with a {1 1 0} surface would be the most reactive. However, the ceria {1 0 0} surface is polar, with a positively charged Ce layer and negatively charged O layers, and is unstable upon heating, relaxing to a low-energy surface. Therefore, the {1 0 0} surface may undergo surface reconstruction with poorer activity, although the {1 0 0} surface itself would have a strong adsorption with CO. The formation of oxygen vacancy was estimated by Raman spectroscopy as shown in Fig. 5. The relative concentration of oxygen vacancies was represented by the area ratio of peaks at 595 and 460 cm^{-1} of the Raman spectroscopy [28,29]. As demonstrated in Fig. 5(d), the oxygen vacancy increased greatly upon copper deposition [30]. When bare ceria were compared, the rods had the most oxygen vacancy, and the cubes had the least oxygen vacancy. However, when the copper was deposited, the Cu/ceria-rods and Cu/ceria-octahedra had comparable oxygen vacancies, although the bare octahedra had an oxygen vacancy as low as the bare cubes. The Cu/ceria-octahedra had an oxygen vacancy comparable to the Cu/ceria-rods, and more copper adsorbed on the surface, resulting in the highest CO conversion at 140 °C.

The shape change of the 4 wt% Cu/ceria was checked after the PROX measurements. Fig. 6(a)–(c) shows TEM images of Cu/ceria before the PROX test and Fig. 6(d)–(f) shows the TEM images after the PROX test. No shape change was observed, nor were distinct copper oxide nanoparticles observed. The removal of surface oxygen by the oxidation reaction and the re-filling of the oxygen vacancy did not change the shape of the ceria nanoparticles significantly. The long-term stability of the PROX reaction was tested over 100 h at 140 °C. As shown in Fig. 7, the Cu/ceria-octahedra showed no degradation over 100 h while the CO conversion decreased from 84% to 73% for the Cu/ceria-rods, from 67% to 46% for the Cu/ceria-cubes, respectively. The stability of the low index plane was estimated to be {1 1 1} > {1 1 0} > {1 0 0} from the theoretical simulation [6]. As expected, the Cu/ceria-octahedra with the {1 1 1} surface showed the best long-term stability. The shape of the catalyst affects not only the activity and selectivity, but also the stability of a long-term reaction.

The effect of the amount of deposited copper was evaluated as shown in Fig. 8. The PROX activity and selectivity were compared for the 1, 4, and 10 wt% Cu/ceria-octahedra. As the copper was deposited on the ceria, the oxygen vacancy and CO adsorption increased, resulting in higher PROX activity. The 4 wt% Cu/ceria showed the best activity. The 1 wt% Cu/ceria seemed to have an insufficient number of active sites for CO oxidation. However, the 10 wt% Cu/ceria showed poorer activity than the 4 wt% Cu/ceria. According to the XRD of the 10 wt% Cu/ceria, separate CuO peaks were observed. Too much CuO on the surface promotes H_2 oxidation, as evidenced by the lower selectivity at low temperatures [31].

Gold and platinum were also deposited on the various shapes of ceria, and their PROX activities were measured as shown in Fig. 9. A 1 wt% of metals was deposited. When a 4 wt% of metals was

deposited, the activity was similar to or lower than the 1 wt% cases. For both Au and Pt cases, the rods showed the highest activity at low temperatures while the activity was similar for rods and octahedra at high temperatures. These noble metals showed higher activity than Cu/ceria at the lower temperature region, but their maximum activity was lower than Cu/ceria, being 84% at 40 °C for Au/ceria and 74% at 80°C for Pt/ceria compared to 95% at 140 °C for Cu/ceria. The surface defects of ceria play a role as anchoring sites of metals [32], and the interactions of the ceria surface defects and the anchored metals would vary for different kinds of metal. Consequently, the PROX properties were greatly affected by the kind of deposited metal.

4. Conclusion

Copper was deposited on different shapes of ceria nanocrystals (rods, cubes, and octahedra). The activity, selectivity and long-term stability of the Cu/ceria catalysts were evaluated for the PROX reaction. When the copper was deposited on the ceria support, the surface content of the copper significantly differed depending on the ceria shapes, with more copper on the octahedra. Copper seemed to incorporate inside the ceria lattice more in ceria rods. The CO adsorption increased greatly upon copper deposition. The Cu/ceria-rods showed greater CO adsorption in high temperatures above 250 °C, whereas the Cu/ceria-octahedra showed slightly more CO adsorption at low temperatures. Copper incorporated inside the ceria lattice would move back to the ceria surface more at high temperatures, resulting in more CO oxidation. The oxygen vacancy increased significantly after copper deposition. The Cu/ceria catalysts showed no apparent shape degradation after the PROX reaction. The high activity of the Cu/ceria-octahedra, especially, remained unchanged over 100 h while the other shapes showed degradation. Au or Pt was also deposited on the different ceria shapes, and their PROX activity and selectivity were evaluated.

Acknowledgements

This work was supported by the DAPA/ADD of Korea, the National Research Foundation of Korea Grant Funded by the Korean Government (MEST) (NRF-2009-C1AAA001-0092926) and the Korean Ministry of Environment as Converging technology project (202-091-001).

References

[1] A.R. Tao, S. Habas, P. Yang, Small 4 (2008) 310.
[2] Y. Xia, Y.J. Xiong, B. Lim, S.E. Skrabalak, Angew. Chem., Int. Ed. 48 (2009) 60.
[3] K.M. Bratlie, H. Lee, K. Komvopoulos, P. Yang, G.A. Somorjai, Nano Lett. 7 (2007) 3097.
[4] S.E. Habas, H. Lee, V. Radmilovic, G.A. Somorjai, P. Yang, Nat. Mater. 6 (2007) 692.
[5] C. Kim, H. Lee, Catal. Commun. 11 (2009) 7.
[6] E. Aneggi, J. Llorca, M. Boaro, A. Trovarelli, J. Catal. 234 (2005) 88.
[7] K.B. Zhou, X. Wang, X.M. Sun, Q. Peng, Y.D. Li, J. Catal. 229 (2005) 206.
[8] M. Nolan, J.E. Fearon, G.W. Watson, Solid State Ionics 177 (2006) 3069.
[9] M. Nolan, G.W. Watson, J. Phys. Chem. B 110 (2006) 16600.
[10] R. Si, M. Flytzani-Stephanopoulos, Angew. Chem., Int. Ed. 47 (2008) 2884.
[11] P. Ratnasamy, D. Srinivas, C.V.V. Satyanarayana, P. Manikandan, R.S.S. Kumaran, M. Sachin, V.N. Shetti, J. Catal. 221 (2004) 455.
[12] W.B. Kim, T. Voitl, G.J. Rodriguez-Rivera, S.T. Evans, J.A. Dumesic, Angew. Chem., Int. Ed. 44 (2005) 778.
[13] C. Rossignol, S. Arrii, F. Morfin, L. Piccolo, V. Caps, J.L. Rousset, J. Catal. 230 (2005) 476.
[14] S. Alayoglu, A.U. Nilekar, M. Mavrikakis, B. Eichhorn, Nat. Mater. 7 (2008) 333.
[15] T. Caputo, L. Lisi, R. Pirone, G. Russo, Ind. Eng. Chem. Res. 46 (2007) 6793.
[16] D. Gamarra, A. Hornes, Z. Koppany, Z. Schay, G. Munuera, J. Soria, A. Martinez-Arias, J. Power Sources 169 (2007) 110.
[17] A. Gomez-Cortes, Y. Marquez, J. Arenas-Alatorre, G. Diaz, Catal. Today 133 (2008) 743.
[18] C.R. Jung, J. Han, S.W. Nam, T.H. Lim, S.A. Hong, H.I. Lee, Catal. Today 93–95 (2004) 183.
[19] F. Marino, C. Descorme, D. Duprez, Appl. Catal. B: Environ. 58 (2005) 175.
[20] A. Martinez-Arias, A.B. Hungria, M. Fernandez-Garcia, J.C. Conesa, G. Munuera, J. Power Sources 151 (2005) 32.
[21] H.X. Mai, L.D. Sun, Y.W. Zhang, R. Si, W. Feng, H.P. Zhang, H.C. Liu, C.H. Yan, J. Phys. Chem. B 109 (2005) 24380.
[22] G. Avgouropoulos, T. Ioannides, Appl. Catal. B: Environ. 67 (2006) 1.
[23] D. Gamarra, C. Belver, M. Fernandez-Garcia, A. Martinez-Arias, J. Am. Chem. Soc. 129 (2007) 12064.
[24] C.S. Polster, H. Nair, C.D. Baertsch, J. Catal. 266 (2009) 308.
[25] X.L. Tang, B.C. Zhang, Y. Li, Y.D. Xu, Q. Xin, W.J. Shen, Appl. Catal. A: Gen. 288 (2005) 116.
[26] Z.X. Yang, B.L. He, Z.S. Lu, K. Hermansson, J. Phys. Chem. C 114 (2010) 4486.
[27] D. Gamarra, G. Munuera, A.B. Hungria, M. Fernandez-Garcia, J.C. Conesa, P.A. Midgley, X.Q. Wang, J.C. Hanson, J.A. Rodriguez, A. Martinez-Arias, J. Phys. Chem. C 111 (2007) 11026.
[28] J. Li, P.F. Zhu, S.F. Zuo, Q.Q. Huang, R.X. Zhou, Appl. Catal. A: Gen. 381 (2010) 261.
[29] Z.Y. Pu, J.Q. Lu, M.F. Luo, Y.L. Me, J. Phys. Chem. C 111 (2007) 18695.
[30] L. Dong, Y. Hu, M. Shen, T. Jin, J. Wang, W. Ding, Y. Chen, Chem. Mater. 13 (2001) 4227.
[31] T. Caputo, L. Lisi, R. Pirone, G. Russo, Appl. Catal. A: Gen. 348 (2008) 42.
[32] Q. Fu, H. Saltsburg, M. Flytzani-Stephanopoulos, Science 301 (2003) 935.